Technical Report

distributed by

Defense Technical Information Center
DEFENSE LOGISTICS AGENCY
Cameron Station • Alexandria, Virginia 22314

UNCLASSIFIED/UNLIMITED

SE

WT-913

This document consists of 34 pages

No. [illegible] of 195 copies, Series A

...ration
...ASTLE

- May 1954

Project 2.2

GAMMA RATE VERSUS TIME

Issuance Date: February 24, 1959

This document contains restricted data as defined in the Atomic Energy Act of 1954. Its transmittal or the disclosure of its contents in any manner to an unauthorized person is prohibited.

HEADQUARTERS FIELD COMMAND, ARMED FORCES SPECIAL WEAPONS PROJECT
SANDIA BASE, ALBUQUERQUE, NEW MEXICO

Inquiries relative to this report may be made to

Chief, Armed Forces Special Weapons Project
Washington, D. C.

When no longer required, this document may be destroyed in accordance with applicable security regulations.

DO NOT RETURN THIS DOCUMENT

AEC Technical Information Service Extension
Oak Ridge, Tennessee

④ NA ⑤ 245150

SECRET

REG. NO. 14584
LOG. NO. 9-5331
WDSOT

③ ISA ⑨ WT---913

OPERATION CASTLE---PROJECT 2.2

Report to the Scientific Director

⑥ GAMMA RATE VERSUS TIME [U]

⑩ by Peter Brown and
Gerald Carp,

U. S. Army Signal Engineering Laboratories
Fort Monmouth, N. J.

⑦ NA
⑧ U
⑨ NA
⑪ May 54,
⑫ 34 p.
⑬ NA
⑭ NA
⑮ NA
⑯ NA
⑰ NA
⑱ S-RD
⑲ NA

LC.

SECRET

GENERAL SHOT INFORMATION

	Shot 1	Shot 2	Shot 3	Shot 4	Shot 5	Shot 6
DATE	1 March	27 March	7 April	26 April	5 May	14 May
CODE NAME (Unclassified)	Bravo	Romeo	Koon	Union	Yankee	Nector
TIME*	06:40	06:25	06:15	06:05	06:05	06:15
LOCATION	Bikini, West of Charlie (Nemu) on Reef	Bikini, Shot 1 Crater	Bikini, Tare (Eninman)	Bikini, on Barge at Intersection of Arcs with Radii of 6900' from Dog (Yurochi) and 3 Statute Miles from Fox (Aomoen).		Eniwetok, IVY Mike Crater, Flora (Elugelab)
TYPE	Land	Barge	Land	Barge	Barge	Barge
HOLMES & NARVER COORDINATES	N 170,617.17 E 76,163.98	N 170,635.05 E 75,950.46	N 100,154.50 E 109,799.00	N 161,698.83 E 116,800.27	N 161,424.43 E 116,688,15	N 147,750.00 E 67,790.00

* APPROXIMATE

ABSTRACT

~~The objective of Project 2.2 was to measure~~ initial- and residual-gamma rates, as a function of time at various distances from high-yield thermonuclear detonations.

Initial-gamma rate versus time was measured at fixed distances from ground zero. In particular, measurements were made of the effect on initial-gamma rate caused by the passage of the shock front from ground zero through the detector station.

Residual-gamma rate versus time was measured to provide gamma-radiation time-intensity data, which give information both on fallout rate of arrival and gamma-field-decay rate during the 36-hour period after the detonation.

Scintillation detectors were used in making measurements. The instrument stations were self-contained---the only outside facilities required were timing signals to turn on the stations at a predetermined time prior to the detonation.

Data obtained indicate that the expanding fireball and the passage of the shock front from ground zero through the detector station had a marked effect on the initial-gamma rate---hence on the integrated exposure. The initial-gamma rate reached its first peak immediately after the detonation, decreased slowly, began to rise slowly, and then increased rapidly to a second peak (which was about the same value as the first peak). After reaching the second-peak value, the initial-gamma rate decreased rapidly to zero.

The slow decrease in initial-gamma rate was attributed to the natural decay of the fission products; the slow rise, to the expanding of the fireball and approach of the shock front; and the rapid increase, to the passage of the shock front through the detector station. These effects were also evidenced in the integrated exposure both prior and subsequent to the arrival of the shock front. The average velocity of the shock front was found to decrease rapidly with distance from ground zero.

The decay exponent from the residual contamination and fallout varied with distance and direction from ground zero, and its absolute value increased rather abruptly several hours after the detonation. This abrupt increase is attributable to the presence of short-lived isotopes in the residual contamination and fallout.

The measurements made by Project 2.2 of initial-gamma radiation exposures from thermonuclear devices of high yield are in good agreement with data from "The Nuclear Radiation Handbook," AFSWP 1100, (Reference 9) (see Figure 4.1).

It appears that the initial-gamma radiation is of negligible significance, because blast and thermal effects in the same distance range are so great by comparison that survival would be possible only if personnel were disposed inside blast- and thermal-proof bunkers.

ABSTRACT

[redacted]

This report is one of the reports presenting the results of the 34 projects participating in the Military Effects Tests Program of Operation Castle, which included six test detonations. For readers interested in other pertinent test information, reference is made to WT-934, "Summary Report of the Commander, Task Unit 13, Programs 1-9," Military Effects Program. This summary report includes the following information of possible general interest: (1) an overall description of each detonation, including yield, height of burst, ground zero location, time of detonation, ambient atmospheric conditions at detonation, etc., for the six shots; (2) discussion of all project results; (3) a summary of each project, including objectives and results; (4) a complete listing of all reports covering the Military Effects Tests Program.

[redacted]

FOREWORD

This report is one of the reports presenting the results of the 34 projects participating in the Military Effects Tests Program of Operation Castle, which included six test detonations. For readers interested in other pertinent test information, reference is made to WT-934, "Summary Report of the Commander, Task Unit 13, Programs 1-9," Military Effects Program. This summary report includes the following information of possible general interest: (1) an overall description of each detonation, including yield, height of burst, ground zero location, time of detonation, ambient atmospheric conditions at detonation, etc., for the six shots; (2) discussion of all project results; (3) a summary of each project, including objectives and results; (4) a complete listing of all reports covering the Military Effects Tests Program.

CONTENTS

FIGURES

TABLES

SECRET

Chapter 1
INTRODUCTION

1.1 OBJECTIVES

The objectives of Project 2.2 were to measure initial- and residual-gamma rates as a function of time at various distances from high-yield thermonuclear detonations.

Prior to Castle, little data had been obtained on the effect of the shock front from high-yield thermonuclear devices on gamma rate and gamma exposure. Project 2.2 was designed to make accurate determination of gamma rates and exposures to be expected at various times and distances from high-yield thermonuclear devices. Comparisons with data obtained from smaller-yield devices may lead to extrapolation factors that would permit more-accurate predictions of radiation levels and dosage over a wide range of yields.

Initial-gamma rate versus time was determined at various fixed distances from ground zero; particularly, the effect on initial-gamma rate caused by the passage of the shock front from ground zero through the detector station.

Residual-gamma rate versus time was measured to provide gamma-radiation time-intensity data, which give information both on fallout rate of arrival and gamma-field-decay rate during the 36-hour period after the detonation.

1.2 BACKGROUND

Predictions of the initial-gamma radiation from high-yield thermonuclear devices had previously been based on [illegible] from relatively low-yield devices or from fragmentary Operation Ivy data (References 1 and 2). Operation Ivy results showed that high-yield devices did not follow the relatively simple scaling laws of [illegible] devices. For devices up to 100 kt, gamma radiation at a given [illegible] scales linearly with yield; for high-yield devices in the megaton range, gamma radiation scales [illegible] with [illegible] yield. This enhancement of initial-gamma radiation was attributed largely to the hydrodynamic effect. The passage of the shock front from the detonation point through the detector station resulted in a [illegible] density

SECRET

RESTRICTED DATA

of the absorption medium, and produced a consequent change in the shape of the gamma-rate-versus-time curves during this period.

1.3 THEORY

The gamma radiation emitted from a nuclear detonation may be divided into two portions: initial and residual radiation. The residual portion may include radiation both from fallout and from neutron-induced activity.

1.3.1 Initial-Gamma Radiation. For devices with yields of less than 100 kt, in which the hydrodynamic effect is small, the initial radiations are divided approximately as shown in Table 1.1 (from Reference 4). The

TABLE 1.1 ENERGY PARTITION AMONG INITIAL RADIATIONS FOR FISSION-TYPE DEVICES

From Reference 4

Mechanism	Percent of Total Fission Energy	Total Energy per Fission
		Mev
Prompt Neutrons	4.0	8
Prompt Gammas*	4.0	8
Fission Product Gammas	2.7	5.4
Fission Product Betas	2.7	5.4
Fission Product Neutrinos	5.5	11
Delayed Neutrons	0.1	0.2

*Mostly absorbed in the device

major contributions to initial-gamma radiation are from the fission-product gammas and from the gamma radiation from neutron capture by N^{14} (n,γ) in the high-explosive components and in air. The prompt gammas are nearly all absorbed in the device itself and are of little significance outside the device. The fission-product gammas predominate at close distances (Reference 4). The N^{14} (n,γ) gammas become increasingly important at greater distances, and eventually become the major contributor. Figure 1.1 shows the contribution from fission-product gammas and N^{14} (n,γ) for a 1-kt surface burst. With respect to time, the N^{14} (n,γ) radiation is essentially emitted within 0.2 second; the fission-product gammas, however, continue to contribute for the first 30 seconds.

For thermonuclear devices, it is necessary to consider the [illegible] reaction of neutrons from the fusion process with N^{14} in addition to gamma radiation from fission-product gammas. The radiation due to the fusion process may vary over wide limits, depending on the design of the device. For a given yield, the number of neutrons available may be [illegible] as great for fusion as for fission, and therefore a large contribution to gamma-radiation exposure may be due to the N^{14} (n,γ) radiation in a thermonuclear device (Reference 3).

1.3.2 Residual-Gamma Radiation. The residual-gamma radiation consists of fission-product radiation from fallout and radiation from neutron-induced activity. The decay rate of the residual radiation from fallout will follow approximately the expression:

$$I_t = I_1 t^{-1.2}$$

and

$$r = \int_{t_1}^{t_2} I_t \, dt = 5I_1 (t_1^{-0.2} - t_2^{-0.2}) \qquad (1.1)$$

Where: I_t = exposure rate at time t

I_1 = exposure rate at unit time

t = time

r = exposure between times t_1 and t_2, where $t_1 \geq 10$ seconds

It is expected that the decay of the residual radiation will vary wit weapon design. For example, the presence of Np^{239} would tend to decrease the absolute value of the decay exponent for a period of time.

<u>1.3.3 Absorption in Air.</u> The absorption of unscattered gamma radiation in homogeneous air is exponential with distance. From a point source of monoenergetic radiation, the variation of intensity with distance is expressed as:

$$I_D = \frac{I_0 \exp(-\mu D)}{4\pi D^2} \qquad (1.2)$$

Where: I_D = intensity at distance D

I_0 = source intensity

μ = total linear absorption coefficient (this coefficient generally decreases with increasing gamma energy)

D = distance

The absorption coefficient μ in Equation 1.2 is applicable for narrow-beam geometry, and a correction should be made for field conditions where the detector is essentially a 4π sensing element. This is done by adding a buildup factor B to Equation 1.2 to account for the scattered radiation that will be detected. Buildup factors for different energies and distances have been calculated (Reference 5), and some values are shown in Table 1.2. For omnidirectional detectors, the expression is:

$$I_D = \frac{I_0 B \exp(-\mu D)}{4\pi D^2} \quad (1.3)$$

1.3.4 Hydrodynamic Effect. As shown in Section 1.3.3, the attenuation of gamma radiation is highly dependent on the amount of absorber between the source and the detector. For devices of less than 100-kt

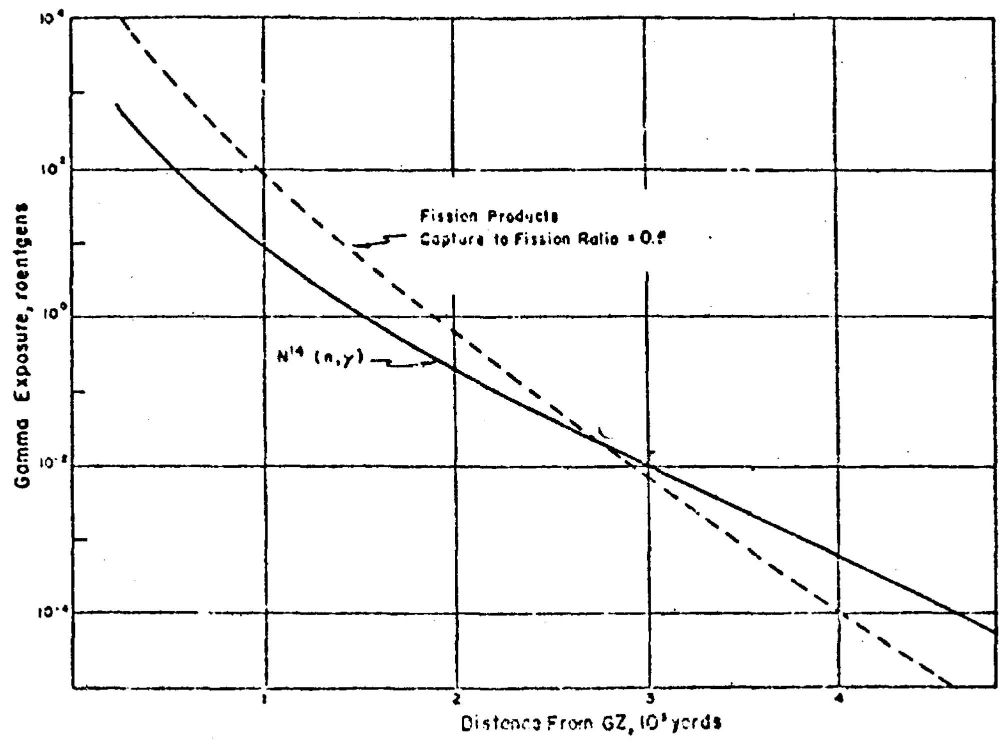

Figure 1.1 Gamma exposure versus distance for a 1-kt surface burst. This illustration shows the contribution from fission-product gammas and N^{14} (n,γ).

yield, essentially all of the initial-gamma radiation is emitted before the shock front can produce an appreciable change in the effective absorption of the air between source and detector. For high-yield devices, the velocity of the shock front is sufficiently high to produce a strong enhancement of a large percentage of the initial-gamma radiation (Reference

6). The higher the yield, the larger is this percentage. A simplified treatment of the hydrodynamic effect follows.

Assuming a sphere of volume V_0, radius R, and filled with a gas of density ρ_0 and mass M, then

$$M = V_0\rho_0 = \frac{4\pi R^3\rho_0}{3} \quad (1.4)$$

Let the gas be compressed into a shell with thickness ΔR (R remaining constant). The new gas volume is expressed as V_1 with a density of ρ_0 ($V_1 = 4\pi R^2 \Delta R$). The mass has not changed; thus

$$M = V_0\rho_0 \doteq 4\pi R^2 \Delta R \rho_1 \qquad (\Delta R << R)$$

$$\frac{4\pi R^3\rho_0}{3} \doteq 4\pi R^2 \Delta R\rho_1 \quad (1.5)$$

$$\Delta R\rho_1 \doteq \frac{R\rho_0}{3} \quad (1.6)$$

Equation 1.6 indicates that a ray originating in the center of the sphere would traverse only a third as much of the mass in the shell model

TABLE 1.2 CALCULATED BUILD-UP FACTORS

The build-up factor (B) given here is the factor B_r (μ_0D, E_0) as computed by the Nuclear Development Associates for AFSWP (Reference 5).

Energy (E_0)	Build-up Factor, B		
	1,000 yards	1,500 yards	3,000 yards
Mev			
1	16.2	29.3	~35
3	3.85	5.35	10.2
4	2.97	4.00	7.00
10	1.70	2.01	2.90

as it would in the homogeneous model. The result would be an enhancement of radiation. Once the shell of material in the shock front passes the detector, an even-greater enhancement should result.

As previously stated, the N^{14} (n,γ) component of initial radiation is essentially emitted within 0.2 second. Since it takes at least one second for the shock front to reach a detector at a distance of 7,000 feet (even for devices in the order of 6 Mt), the N^{14} (n,γ) component is not significantly enhanced. The fission-product gammas continue to contribute during the first 30 seconds; therefore, this radiation is strongly enhanced by the shock wave.

Chapter 2
PROCEDURE

2.1 INSTRUMENTATION

A low-sensitivity system was used for measuring high-initial- and high-residual-gamma radiation rates. For measuring lower residual-gamma radiation rates from fallout, the instrumentation was of high sensitivity. (See Appendix for circuit theory of the instrumentation.)

2.1.1 Low-Sensitivity System.

The detecting element was a stilbene crystal mounted in a graphite block for electron equilibrium. This crystal assembly was installed inside a blast-resistant housing at the top of a light pipe. The crystal output passed through the light pipe and was detected by a 1P21 photomultiplier tube. This tube was used in a 100-percent feed-back circuit, which held the anode current nearly constant (regardless of the incident light) by reducing the photomultiplier-tube dynode voltage. The gain of the tube was approximately a direct function of the antilog of the dynode voltage. In this manner, a useful dynamic range of about 10^9 was realized.

Two different recording systems were used to take advantage of the wide dynamic range of the instrument. Initial-gamma rates from 10^3 r/hr to 10^9 r/hr were recorded by a high-speed recorder, which was capable of resolving to 0.01 second with a recording time to 20 minutes. This recorder, manufactured by the Sanborn Company, Cambridge, Massachusetts, used heat-sensitive paper and a hot-wire stylus. It was found to be well-suited to recording under the adverse conditions encountered during nuclear tests, since it was virtually free of the troubles that may arise with ink and photographic recorders.

Initial-gamma rates from 0.20 r/hr to 10^4 r/hr with low resolution over a long-time period were recorded by a Bristol recording millivoltmeter. This recorder used smoked paper, had a running time of about 24 hours, and a time resolution that was proportional to the running time (1 minute at the start and 5 minutes at the end of 24 hours).

A double station, consisting of two detectors, one with a low- and one with a high-resolution recording system, covered the range from 0.2 r/hr to 10^9 r/hr and recorded useful data from 0.01 second to 24 hours.

2.1.2 High-Sensitivity System.

The detecting element was an anthracene crystal mounted in a graphite block for electron equilibrium and attached to the window of a 5819 photomultiplier tube. This tube, like the 1P21 mentioned in Section 2.1.1, was used in a 100-percent feed-back circuit, and the anode current was kept virtually constant. Its gain was approximately a direct function of the antilog of the dynode voltage.

Therefore, it was possible to plot the incident light, or gamma radiation, as a function of the dynode voltage.

All electronics were mounted inside a light-aluminum housing for protection from weather, thermal influences, and small blast pressures. The output was recorded on a Bristol recording millivoltmeter, which recorded gamma rates from 0.2 r/hr to 10^4 r/hr for a period from 1 minute to 24 hours.

For field installations, the instrumentation systems described in Sections 2.1.1 and 2.1.2 were mounted inside standard 55-gallon steel drums imbedded in concrete. Figure 2.1 is a block diagram of the detector systems.

2.1.3 Special Detector System. A special detector system was designed and constructed to determine the effects of high-gamma rates and

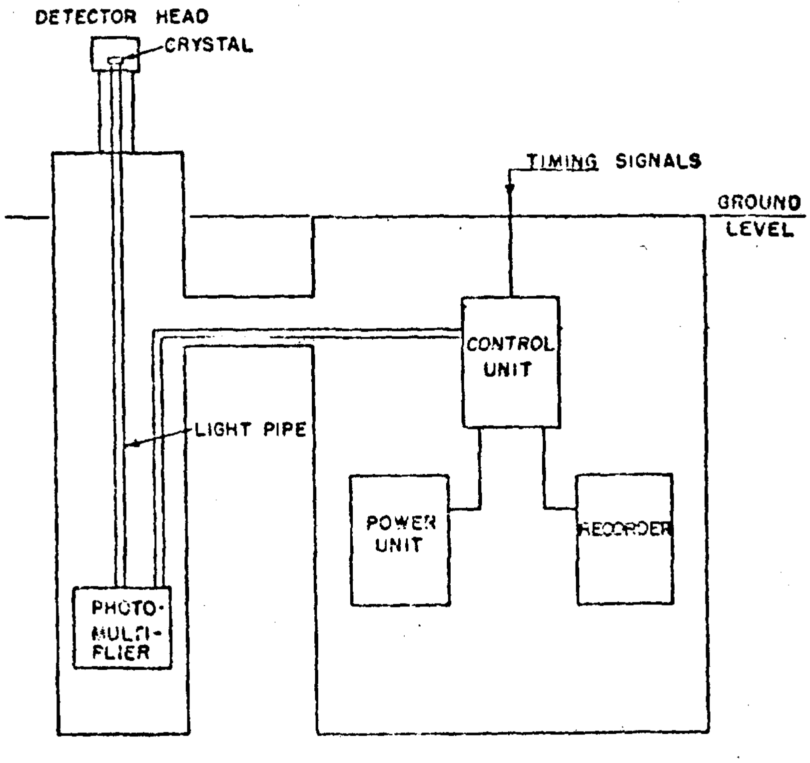

Figure 2.1 Block diagram of a typical detector system. The detecting element is either a stilbene or an anthracene crystal depending on whether it is part of a low- or a high-sensitivity system.

cumulative exposures on the crystal detecting element. Two low-sensitivity detector heads were employed: one in normal usage and the second covered with a 5-inch-thick layer of lead shot to attenuate the gamma radiation reaching the crystal by a factor of about 100. The "normal" head detected the incident gamma rate, while the lead-covered one detected 1/100 of this rate, and also received only 1/100 of the total exposure.

To calibrate the station with the normal head, the first method was used as described in Section 2.2.1. This required the placement of a density-four neutral filter between the crystal and the photomultiplier tube of the normal station to increase the range to 10^8 r/hr. The lead-covered head required only a density-two neutral filter, inasmuch as the lead covering served to attenuate the incident gamma radiation by a factor of 100 (equivalent to a density-two filter).

If the two detector heads track, the crystals are not being differentially affected by gamma rates and cumulative exposures. If the detectors do not track, it is an indication that there is a rate or cumulative exposure dependence of the system or a significant change in the spectral quality of incident radiation. In the event that scintillation crystals are shown to be neither rate nor dosage dependent, the assumption may be made that a nearly linear extrapolation of low-intensity calibration can be performed.

2.2 CALIBRATION

2.2.1 <u>High-Intensity Calibration.</u> Calibration for high rates was based on the assumption that the light output of the scintillation crystal is a linear function of the incident radiation at least up to 10^8 r/hr.

Two techniques were used to calibrate the high-level instruments. In the first method, the detector head was calibrated from 0.2 r/hr to 10^4 r/hr, using an 88-curie Co^{60} source. To extend the range of the instrument to 10^8 r/hr, a density-four neutral filter was placed between the crystal and the photomultiplier tube. Effectively, the system would then measure radiation from about 0.2×10^4 r/hr to 10^8 r/hr.

It was necessary to put shielding around the photomultiplier tube, since it was sensitive to radiation. The purpose of the shielding was to attempt to attenuate the incident gamma radiation on the photomultiplier by the same order of magnitude as the neutral density filter attenuates the light from the crystal. (This was not possible in the field, as the amount of scatter radiation striking the photomultiplier through the light pipe precluded an attenuation factor greater than 10^3.)

In the second high-intensity calibration method, the detector head was first calibrated from 0.2 r/hr to 10^4 r/hr using an 88-curie Co^{60} source. The crystal was then replaced by a light source of the same spectral quality as the stilbene crystal output. The output of this light source could be varied in known increments. A plot was made of this output versus the relative incident luminous flux. The calibration curve thus obtained was then normalized to the curve obtained with radiation and was found to track very closely up to the maximum of 10^4 r/hr (Figure 2.2). Because of the agreement between the light and the radiation calibrations at the low levels, the light calibration was used as a basis for extrapolating the radiation calibration curves up to 10^9 r/hr.

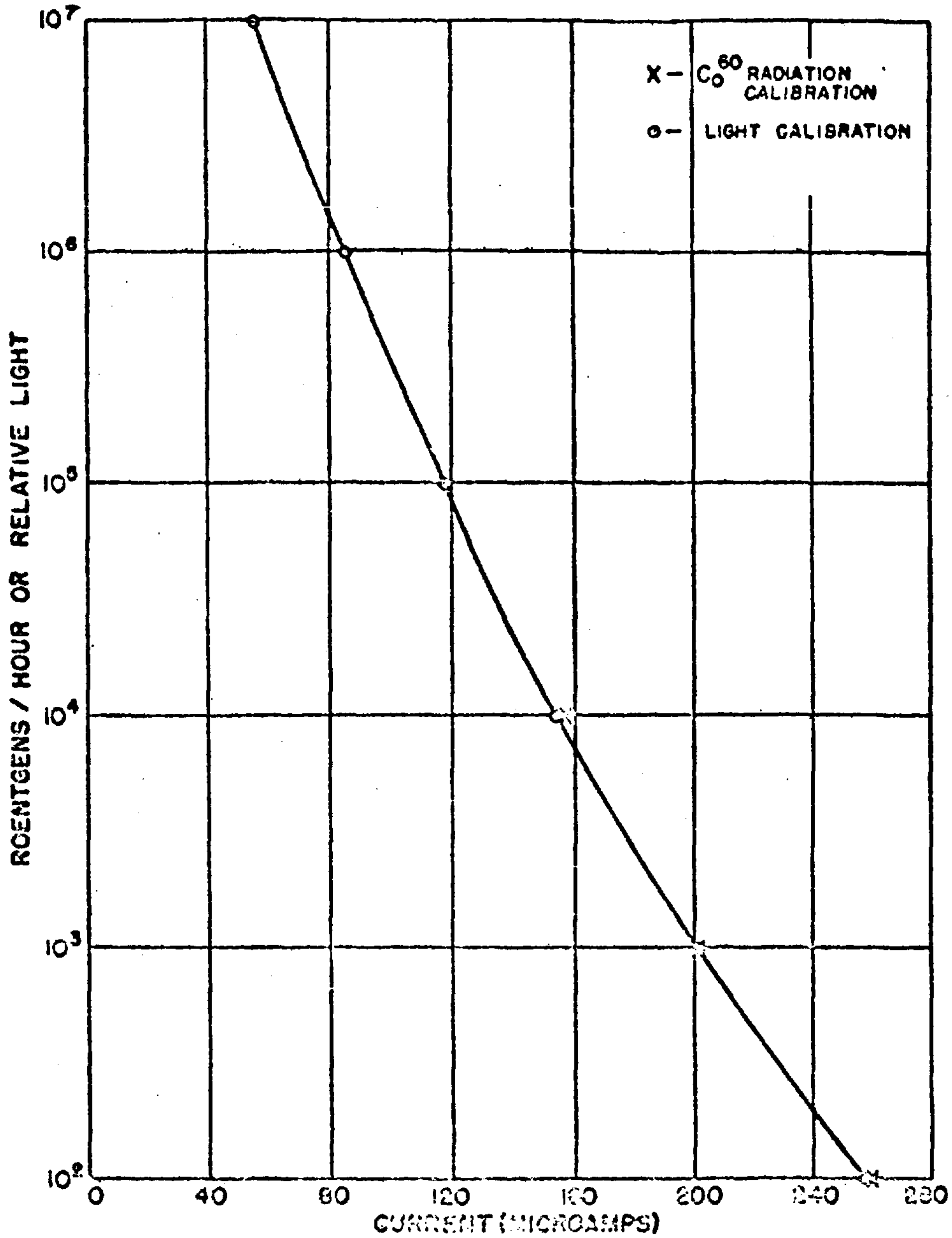

Figure 2.2 Calibration curve for the second high-intensity calibration method. It represents plots of the radiation rate and relative light versus detector output.

TABLE 2.1 INSTRUMENTATION FOR EACH SHOT

Station Number	Island Location	Range from Zero	Description
		feet	
Shot 1:			
220.08	Oboe	83,762	Single high-sensitivity unit
220.10	Able	6,400	Two low-sensitivity units
220.11	Charlie	7,706	Two low-sensitivity units
220.12	Dog	41,372	Two low-sensitivity units with one detector head shielded with Pb
220.13	Easy	45,279	Single high-sensitivity unit
220.14	Peter	82,645	Single high-sensitivity unit
221.01	William	61,719	Single high-sensitivity unit
221.02	Yoke	54,480	Single high-sensitivity unit
221.03	Zebra	50,598	Single high-sensitivity unit
221.04	Alfa	49,432	Single high-sensitivity unit
221.05	Bravo	47,590	Single high-sensitivity unit
Shot 2:			
220.08	Oboe	~83,800	Single high-sensitivity unit
220.12	Dog	~41,400	Single high-sensitivity unit
220.14	Peter	~82,700	Single high-sensitivity unit
Shot 3:			
220.08	Oboe	16,778	One low- and one high-sensitivity unit
220.09	Roger	7,511	One low- and one high-sensitivity unit
220.12	Dog	69,112	Single high-sensitivity unit
220.14	Peter	11,779	One low- and one high-sensitivity unit
Shot 4:			
220.06	Fox	13,501	One low- and one high-sensitivity unit
220.07	George	15,579	One low- and one high-sensitivity unit
220.12	Dog	7,171	Two low-sensitivity units
220.13	Easy	9,602	One high-sensitivity unit
Shot 5:			
None			
Shot 6:			
Unnumbered	Alice	~18,000	Two portable high-sensitivity units

2.2.2 Low-Intensity Calibration. The low-level detectors for measuring fallout were calibrated directly with an 88-curie Co^{60} source.

2.2.3 Energy Dependence. Both the anthracene and stilbene detector systems gave approximately linear response over the energy range from 100 kev to 5 Mev. The postoperation laboratory recalibration of the anthracene and stilbene detectors that was originally planned could not be done.

2.3 SHOT PARTICIPATION

Table 2.1 summarizes the location, range, and types of instrumentation used in each of the shots.

TABLE 3.1 GAMMA RADIATION DATA

Station	Type	Distance to Ground Zero	Azimuth	Gamma Exposure: Prior to Arrival of Shock Front		Gamma Exposure: Subsequent to Arrival of Shock Front		Integrated	Maximum Rate	Decay Exponent x ($R_t = R_1 t^{-x}$)	Comments
		feet	deg min	r	Percent of Integrated	r	Percent of Integrated		r/hr		
Shot 1:											
220.11 Charlie	High Intensity	7,206	83 24	9,900	---	---	---	9,900 (0.9 sec)	6×10^7	---	Initial radiation received to time of arrival of shock front. Residual detector destroyed.
220.03 Oboe	Fallout	83,762	138 45	---	---	---	---	133 (0.25 to 20 hr)	34	0.81 (1 to 18 hr)	
220.12 Dog	Fallout	41,372	92 28	---	---	---	---	3,735 (0.25 to 20 hr)	1,000	1.35 (3 to 10 hr) 2.1 (10 to 24 hr)	
Shot 3:											
220.12 Dog	Fallout	69,112	83 24	---	---	---	---	51 (0.33 to 15 hr)	24	1.28 (1 to 12 hr)	
		feet	deg min	r	Percent of Integrated	r	Percent of Integrated		r/hr		
Shot 4:											
220.12 Dog	High Intensity	7,171	5 34	742 (0.02 to 1.3 sec)	6.4	12,421 (1.3 to 20 sec)	93.6	13,263 (0.02 to 20 sec)	7.2×10^6	---	Initial radiation received in entirety. Residual records destroyed by water.
220.06 Fox	High Intensity	1[illegible],501	48 11	10.5 (0.02 to 4.5 sec)	11	80.6 (4.5 to 25 sec)	89	91.1 (0.02 to 25 sec)	5.2×10^4	---	Initial radiation received in entirety. Residual records destroyed by water.
220.07 George	Fallout	15,579	64 47	---	---	---	---	1,237 (Res) (0.033 to 10 hr)	620 (Res)	1.39 (2 to 6 hr) 1.61 (7 to 10 hr)	Residual radiation recorded. Initial too low to record accurately but probably on the order of 10^3 r/hr.

decay exponent x, in the expression $I_t = I_1 t^{-x}$, was found to change from about 1.35 during the period H + 3 to H + 10 hours to about 2.1 during the next fourteen hours.

Figure 3.2 shows that at Station 220.08, fallout started to build up about 15 minutes after the detonation and reached a maximum rate of 34 r/hr. The integrated exposure was 133 r during the first 24 hours. The decay exponent was 0.81 for the period H + 1 to about H + 18 hours.

Because of the unexpected high yield of Shot 1, the instrumentation sustained serious damage. Low-sensitivity Station 220.10 on Able was destroyed by blast. Fallout Stations 221.05 on Bravo, 221.04 on Alfa,

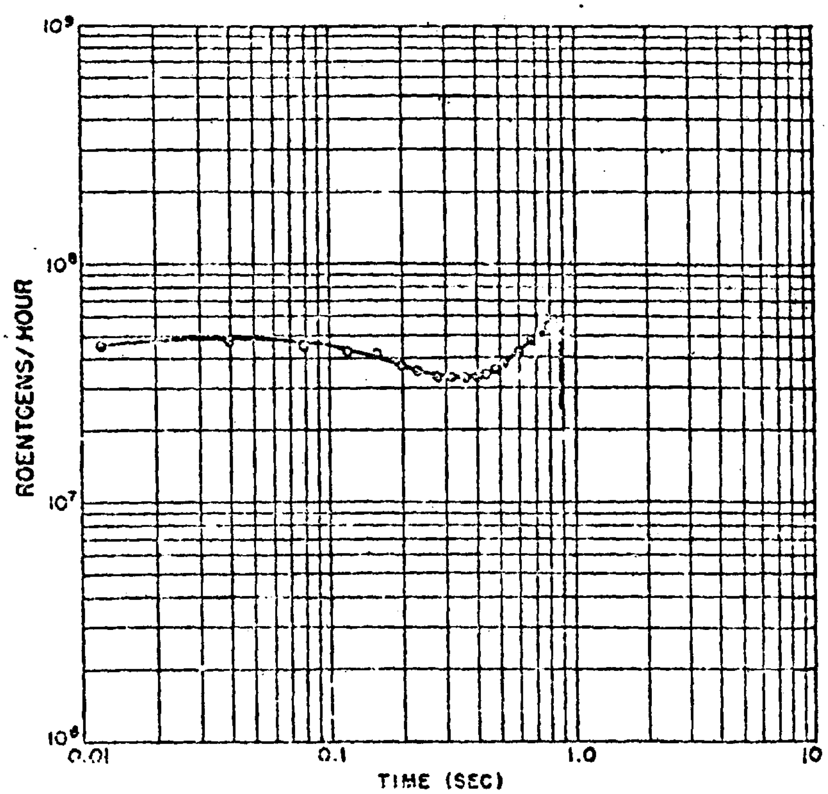

Figure 3.1 Initial-gamma rate versus time for Shot 1, Station 220.11 on Charlie. This station was 7,206 feet from ground zero.

221.03 on Zebra, 221.02 on Yoke, and 221.01 on William either were struck by missiles or inundated by water. These stations did not provide reliable records.

3.1.2 Shot 2. Instrument stations at Able and Charlie were destroyed by high overpressures from Shot 1; therefore, Shot 2 could not be instrumented for close-in initial-gamma-rate measurements. Fallout from

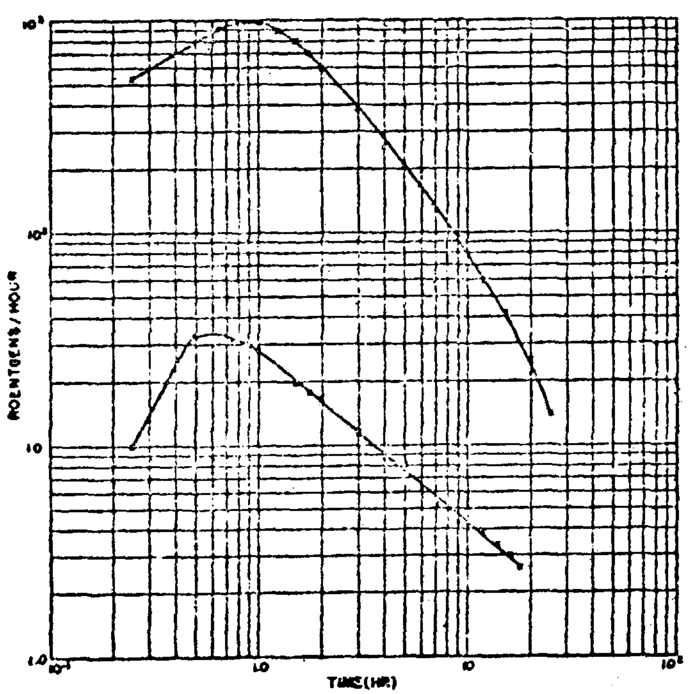

Figure 3.2 Residual-gamma rate versus time for Shot 1, Stations 220.12 on Dog, upper curve; and 220.06 on Oboe, lower curve. These stations were 41,372 feet and 83,742 feet from ground zero, respectively.

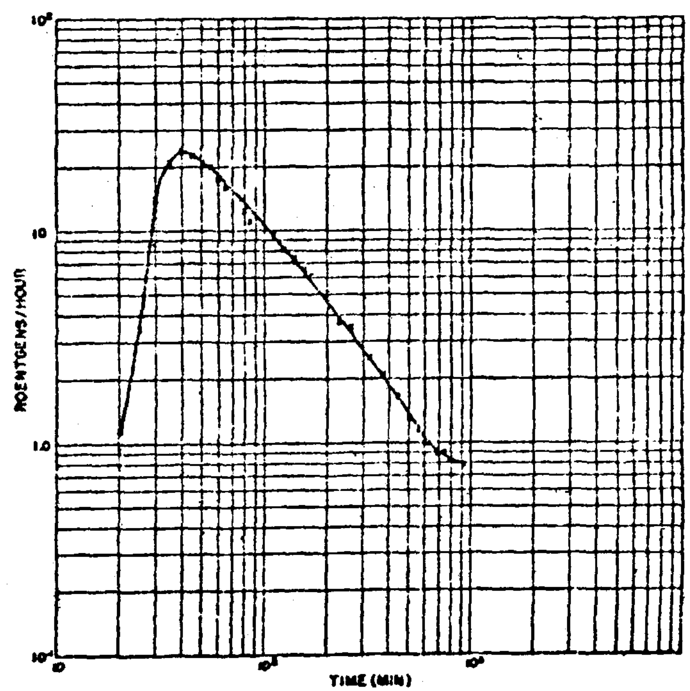

Figure 3.3 Residual-gamma rate versus time for Shot 3, Station 220.12 on Dog. This station was 69,112 feet from ground zero.

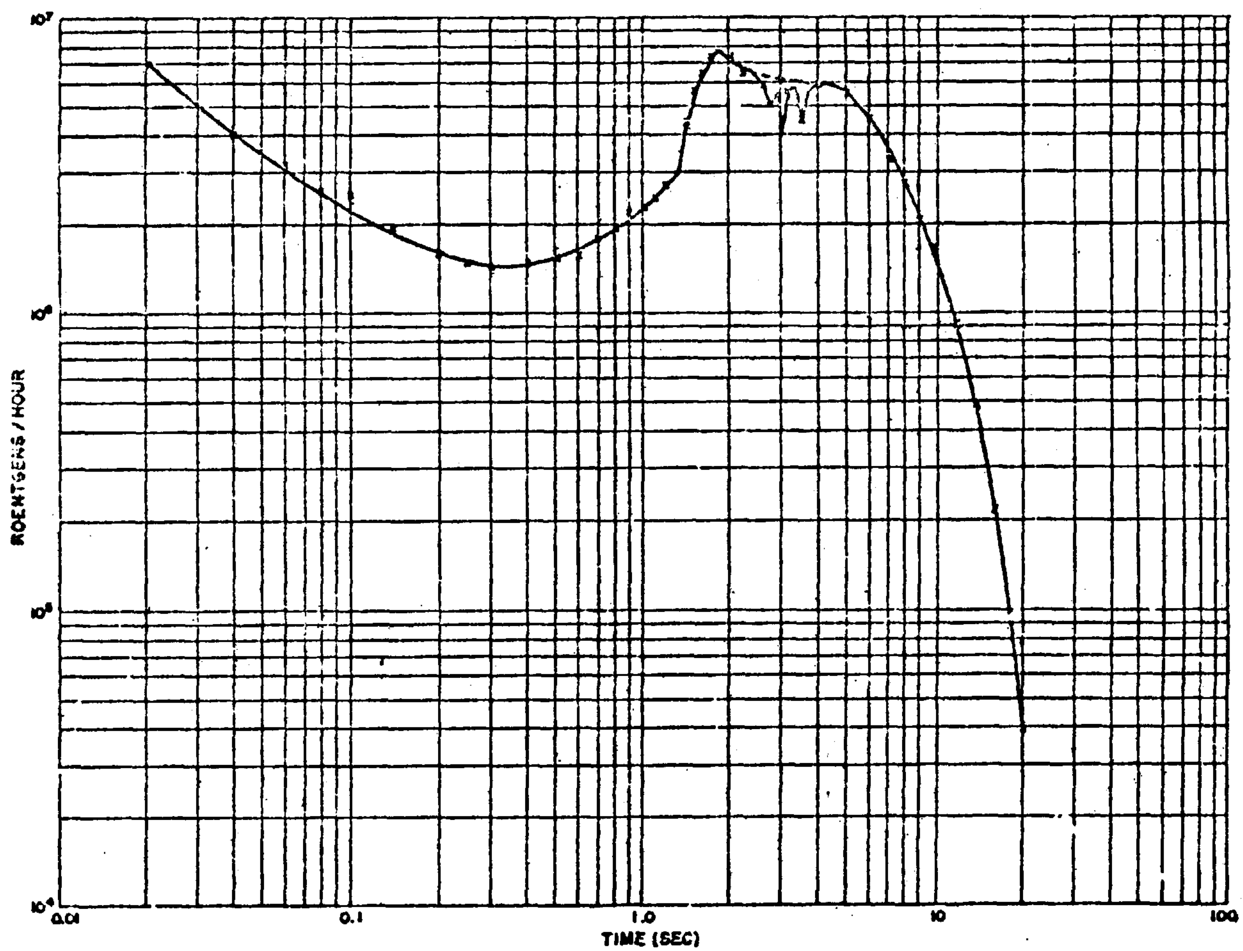

Figure 3.4 Initial-gamma rate versus time for Shot 4, Station 220.12 on Dog. This station was 7,171 feet from ground zero.

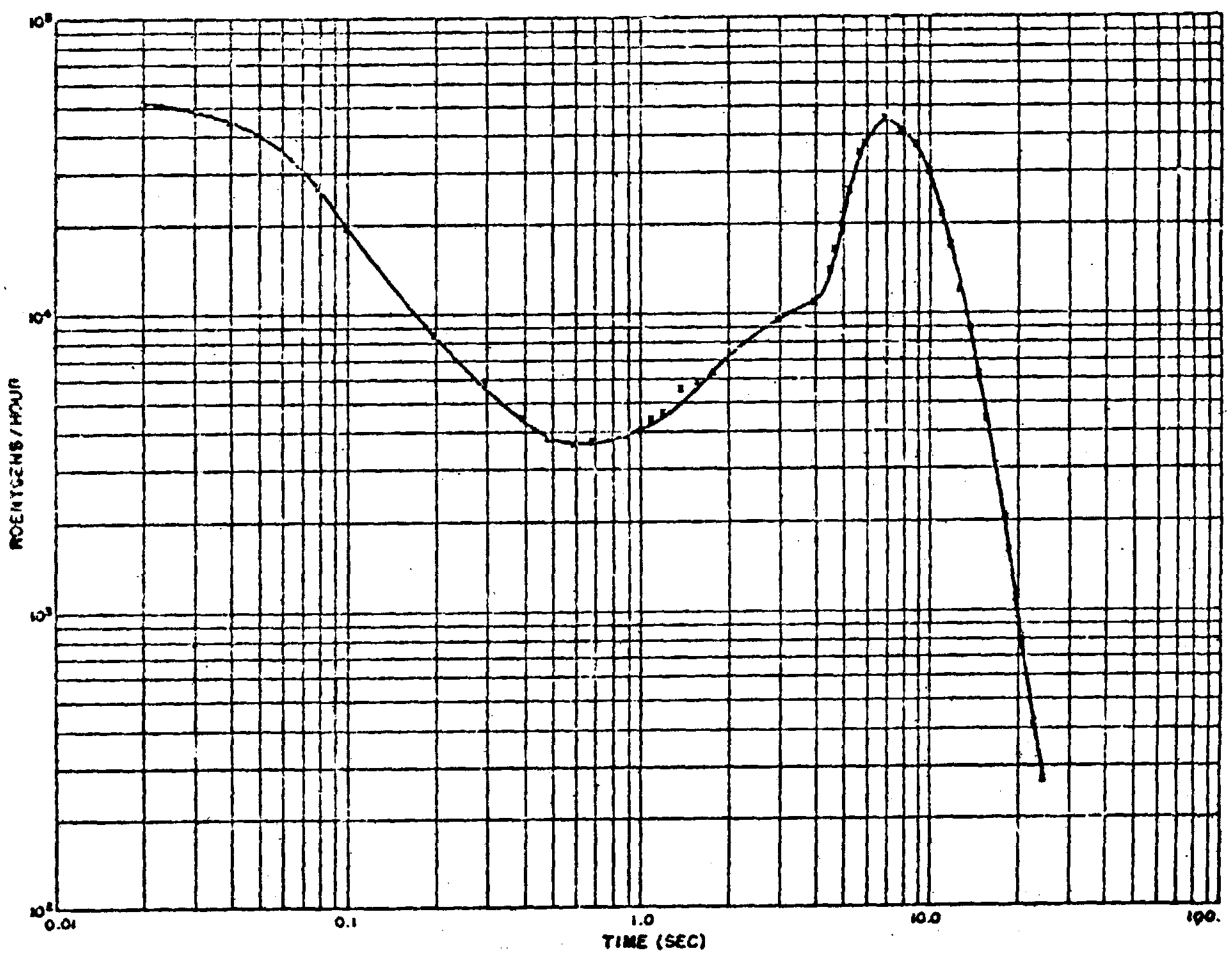

Figure 3.5 Initial-gamma rate versus time for Shot 4, Station 220.06 on Fox. This station was 13, 501 feet from ground zero.

Shot 2 was of such a low level compared to existing background that fallout stations on Oboe, Dog, and Peter did not obtain good records.

3.1.3 Shot 3. No initial-gamma rate data were obtained because of the unexpected low yield of Shot 3. Fallout Station 220.12 on Dog provided a good record (see Figure 3.3). Fallout started to build up about 20 minutes after the detonation and reached a maximum of 24 r/hr. Integrated exposure was 51 r in the first 15 hours. The decay exponent was 1.28 for the period H + 1 to H + 12 hours.

3.1.4 Shot 4. Figure 3.4 (Station 220.12 on Dog) shows that the initial-gamma rate first dropped in magnitude, then increased slowly from 0.4 to about 1.2 seconds, and then increased relatively rapidly to a value of 7.2×10^6 r/hr, approximately the same as the original rate at time of detonation. The slow increase appears to be the combined result of the expansion of the fireball and the approach of the shock front toward the detector station. The rapid increase was caused by the passage of the shock front through the detector station.

Figure 3.5 (Station 220.06 on Fox) shows the same phenomena as Figure 3.4. The expanding fireball and the approach of the shock front cause a slow increase in the gamma rate from 0.7 to 4.48 seconds. Passage of the shock front through the detector station causes an abrupt increase to about 4.5×10^1 r/hr, after 7 seconds. This peak is about the same as the original rate at time of detonation.

The record obtained from Station 220.07 on George shows an initial-gamma spike and the arrival of the shock front 5.86 seconds later. However, the deflection was too small to permit the readout of a time history of the initial gamma. From Shot 4 data, the average velocities of the shock front between ground zero and Dog, Fox, and George are computed to be about 5,100, 3,000, and 2,600 ft/sec, respectively.

Residual-gamma rate versus time is plotted in Figure 3.6 (Station 220.07 on George). Fallout reached a peak value of 620 r/hr, and the recorded exposure of the first 10 hours after detonation was 1,237 r. During the period H + 2 to H + 6 hours, the decay exponent was 1.39, and from H + 7 to H + 10 hours it was 1.61.

These figures represent the data as read; no correction for air density has been made. The relative air density for the Castle events is 0.9.

3.2 DATA CORRELATION

3.2.1 Integrated Exposure Rate Versus Total Exposure. The dosages obtained by integrating the curves of Figures 3.2 and 3.6 have been compared to dosage measurements made by the National Bureau of Standards (NBS) type photographic dosimeters on Project 2.1 at the same station locations (Reference 8). The results are summarized in Table 3.2. Because the gamma rates obtained are valid at a sufficient number of medium-distance stations where exposure did not exceed 10^4 r, it may be assumed that the results are also valid at close-in stations where the total ex-

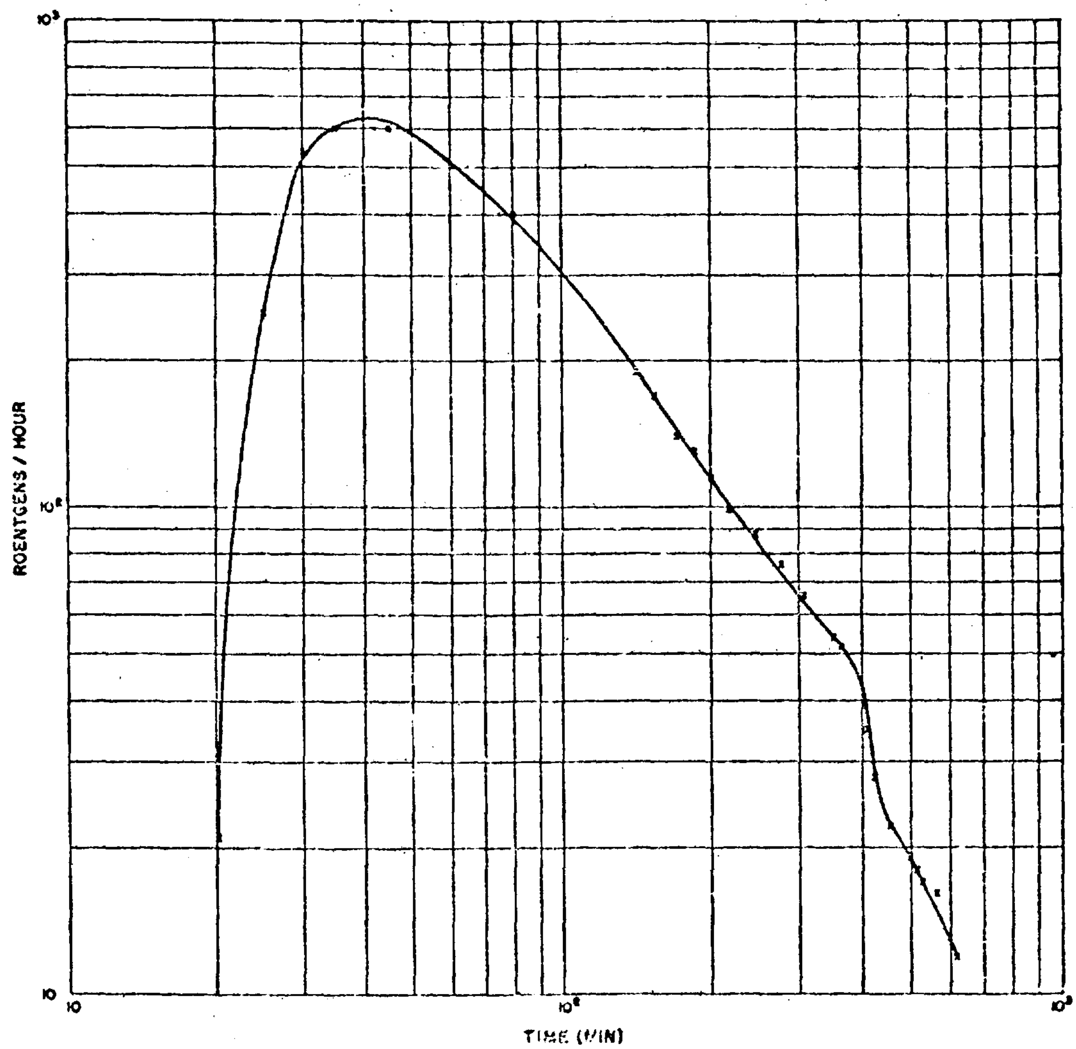

Figure 3.6 Residual-gamma rate versus time for Shot 4, Station 220.07 on George. This station was 15,5[illegible]9 feet from ground zero.

posure was less than 10^8 r. This assumption is based on data showing that the response of scintillation-type crystals is not adversely affected by total exposures of less than 10^8 r (Reference 7).

3.2.2 Special Detector System. The data from Station 220.11 on Charlie, Shot 1, showed that the two heads did not track. This was attributed to the presence of scattered radiation that entered the shielded area through the light pipe. The sensitivity of the photomultiplier tube to radiation required the presence of shielding to attenuate the radiation in the same order of magnitude as the neutral-density filter. When it proved impractical to increase the shielding, the use of neutral-density filters to increase the detector's upper limit was abandoned for remaining shots.

TABLE 3.2 GAMMA RADIATION DOSAGE

Comparison of dosage measurements made with NBS type photographic dosimeters on Project 2.1 and dosage measurements at same ranges made by scintillation detectors on Project 2.2.

Distance to Ground Zero	Project	Station	Dose	Time
feet			r	hr
Shot 1:				
83,762	2.1	210.23	180	H + 82
	2.2	220.08	133	H + 20
41,372	2.1	210.12	6,000	H + 78
	2.2	220.12	3,735	H + 20
Shot 4:				
15,579	2.1	210.21	2,060	H + 104
	2.2	220.07	1,237	H + 10

Chapter 4
CONCLUSIONS

The following conclusions were reached, based on the empirical results of Project 2.2, and on collateral data obtained from other Castle projects:

The passage of the shock front from ground zero to and through the detector station has a marked effect on the initial-gamma radiation rate for high-yield weapons. The percentage of total-initial-gamma-radiation exposure received prior and subsequent to the arrival of the shock front was found to be a function of the distances from ground zero.

Initial-gamma radiation is of negligible significance since blast and thermal effects in the same range of distances are so great that survival would be possible only if personnel were disposed inside blast- and thermal-proof bunkers.

The rate of decay of the residual field radiation from fallout was found to vary with distance and direction from ground zero. The rate of decay increases rather abruptly several hours after the detonation. This may be attributed to the presence of short-lived isotopes in the residual contamination and to fractionalization of fallout materials.

Figure 4.1 indicates that Project 2.2 measurements of initial-gamma radiation exposures from thermonuclear devices of high yield are in good agreement with data from "The Nuclear Radiation Handbook," AFSWP 1100. It should be noted, however, that the Castle Project 2.2 data was one of the sources used in the preparation of the prediction curves of that handbook.

Chapter 3
RESULTS and DISCUSSION

3.1 GENERAL

Figures 3.1 to 3.6 are plots of gamma rate versus time at various distances from ground zero.

Examination of the figures makes apparent the effect of the shock-front passage between ground zero and the detector station during the initial-gamma radiation. After the passage of the shock front, the initial-gamma rate rose almost to the same value as it was at the time of detonation.

Table 3.1 summarizes the gamma-radiation data for the stations used during Shots 1, 3, and 4. The extensive instrumentation originally planned was not followed because of the unexpected loss of most of the equipment stored on Tare during Shot 1. Out of a total of 30 low- and 5 high-sensitivity instruments, only seven of the former and two of the latter were salvaged for succeeding shots.

3.1.1 Shot 1. Figure 3.1 shows initial-gamma rate versus time for Station 220.11 on Charlie. The increase in rate from 0.35 to 0.9 second was apparently caused by the expanding fireball and the approach of the shock front toward the detector station. The shock front arrived at the detector station at 0.9 second. The average velocity of the shock front between ground zero and the detector station was computed to be about 8,000 ft/sec. No further data were obtained because the station was destroyed by missiles at that time.

The special detector system at Station 220.11 on Charlie was designed to determine the rate or cumulative exposure dependence of the crystal detecting elements, as well as to measure the initial-gamma rate. Records obtained showed that the two detector heads did not track. However, it was determined that this was not due to a rate or dosage dependence of the crystals, but rather to scattered gamma radiation entering through the light pipe and striking the photomultiplier tube in the station without a shield around the detector head. Since a density-four neutral filter was placed between the crystals and the photomultiplier tube to increase the range to 10^8 r/hr, the effect of the scattered radiation entering through the light pipe was to multiply the direct effect of gamma radiation on the photomultiplier by several orders of magnitude. Because of this, the record went off scale immediately and gave no true indication of the gamma rate. The station with the shielded detector head provided a good record, because the lead shielding effectively attenuated the gamma radiation that reached the phototube by a factor of 100.

Figure 3.2 plots residual-gamma rate versus time for Stations 220.12 and 220.08. The graph shows that at Station 220.12, fallout started to build up 15 minutes after the detonation and reached a maximum rate of 10^3 r/hr. The integrated exposure for the first 24 hours was 3,735 r. The

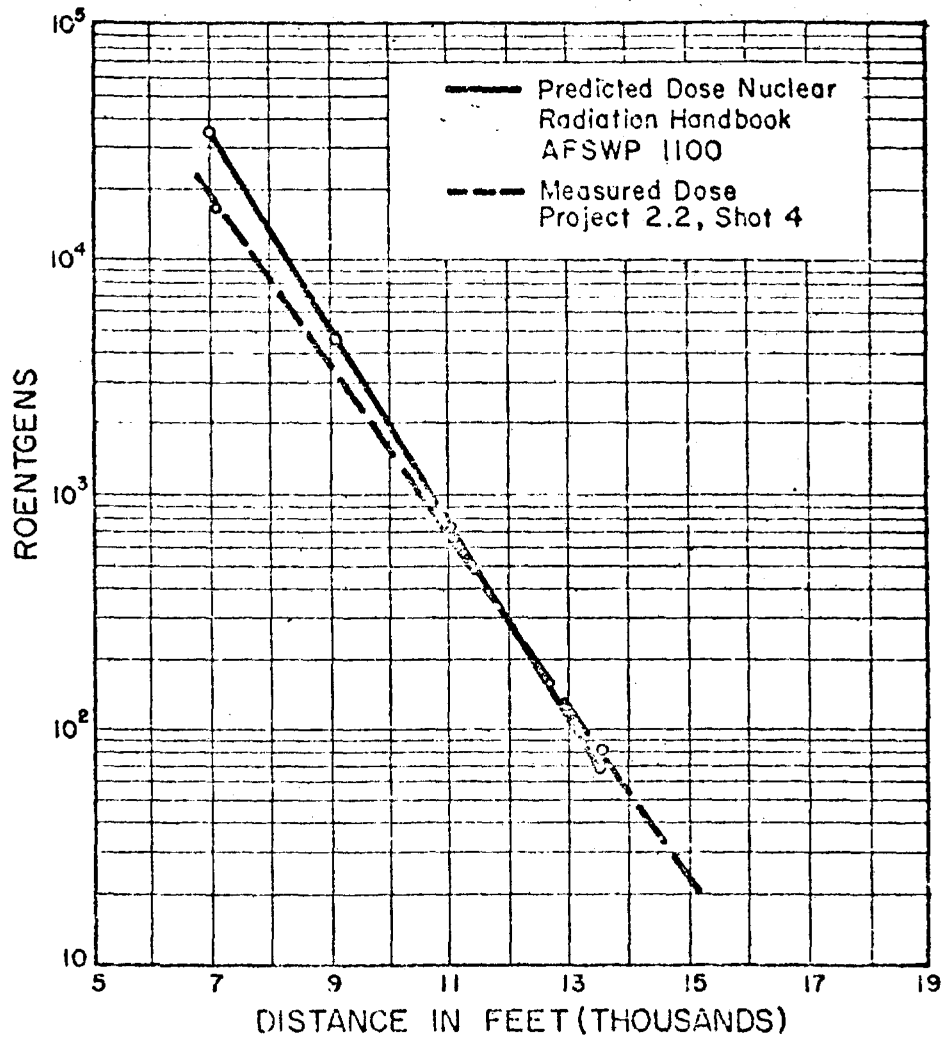

Figure 4.1 Initial-gamma dose versus distance. Comparison of dose measured on Shot 4 with dose computed by method given in The Nuclear Radiation Handbook, AFSWP 1100. Yield 7.0 Mt. Relative air density 0.9.

Appendix

THEORY OF INSTRUMENT OPERATION

Fulfillment of the objectives of this project required an instrument of known operational characteristics in very-high radiation fields, and with an extremely large dynamic range. The former requirement indicated that a scintillation detector would be best suited; the latter led to the choice of a feed-back circuit that kept the photomultiplier-tube anode current substantially constant and thus prevented fatigue of the photocathode under high flux.

The photomultiplier dynode voltage is developed across the cathode resistor of a cathode follower, whose input signal is derived from the photomultiplier anode current (Figure A.1). An increase in the incident luminous flux on the photocathode tends to increase the photomultiplier-

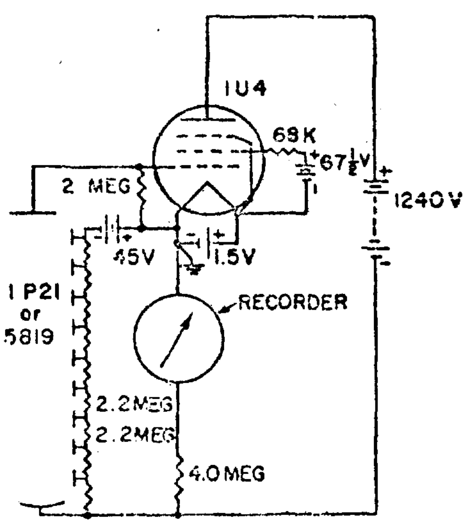

Figure A.1 Schematic diagram of a typical detector system. High-intensity measurements were made with a 1P21 photomultiplier tube whereas fallout measurements were made with a 5819-type tube.

tube anode current. Increased anode current presents a negative signal to the control tube, increasing the impedance of that tube and lowering the voltage across the photomultiplier-tube dynodes. Since the amplification of the photomultiplier tube is a function of dynode voltage, the lowered dynode voltage will cause a decreased anode current. An equilibrium condition is reached at a point where a small increase in photomultiplier anode current decreases the dynode voltage and the gain of the tube to a value that is just enough to keep the anode current at the new level of higher-incident light flux. The output is taken from the cathode of the control tube and fed to a recording voltmeter.

The range of anode-current variation can be calculated for a given control tube and feed-back resistor. If the control tube has a grid bias of 5 volts (that is, the tube cuts off at

-5 volts), and the feed-back resistor is 100 megohms, the maximum value of the anode current I_a is given by:

$$I_a = \frac{E}{R} = \frac{5}{10^8} = 5 \times 10^{-8} \text{ amperes } (0.05\ \mu a)$$

Thus, in a typical circuit the photomultiplier-tube anode current cannot exceed 0.05 μa, and at this value of current there is no danger of photocathode fatigue. Since this was a 100-percent feed-back circuit, it was virtually independent of control-tube characteristics and depended only on the photomultiplier-tube characteristic and the value of the feed-back resistor. The response curve of the instrument closely followed the photomultiplier tube's gain characteristic for varying dynode voltage.

The tube complement included a 1U4 as control, a 1P21 photomultiplier in the low-sensitivity (high-intensity measurements) system, and a 5819 photomultiplier for fallout measurements (high-sensitivity system). Although the rated plate-to-filament voltage of the 1U4 was exceeded by a factor of ten, no difficulties were experienced if filaments were allowed to warm up before applying the plate voltage. A 45-volt battery applied a constant voltage between anode and ninth dynode of the photomultiplier, since the latter is most stable when operated with a constant voltage between those points.

No variation in instrument characteristics could be detected when the control tubes were replaced. This was true even when tubes were tried with different characteristics (such as the 1U4) but similar pin connections. This substantiates the theory that in this 100-percent feed-back circuit, the photomultiplier-tube characteristic is independent of the control-tube parameters. The dynamic range of the instrument is approximately 10^3. When the extreme value of dynamic range is not required, the recorder may be adjusted to operate over a portion of the range, thus providing an expanded scale over the region of interest. For example, in some locations where a dynamic range of 10^2 was sufficient, the recorder was adjusted to operate over this portion of the instrument's output. A more-accurate recording was provided by making these adjustments.

REFERENCES

1. "Super Effects Handbook"; Preliminary Estimates, 2d Revised Edition, Dec 1953; Secret Restricted Data.

2. J. S. Malik; "Preliminary Gamma-Ray Intensity Data"; Operation Ivy, Mike Shot Report; Secret Restricted Data.

3. "Super Effects Handbook"; AFSWP 351, May 1952; Secret Restricted Data.

4. M. G. Schorr and E. S. Gilfillan; "Predicted Scaling of Radiological Effects to Operational Weapons"; Project 2.0, Operation Jangle, WT-391, Jun 1952; Technical Operations Incorporated, Arlington, Massachusetts; Secret Restricted Data.

5. D. C. Borg and C. Eisenhauer; "Spectrum and Attenuation of Initial Gamma Radiation from Nuclear Weapons"; AFSWP 502B, Jan 1955; Weapons Effects Division, Headquarters, Armed Forces Special Weapons Project, Washington, D. C.; Secret Restricted Data.

6. J. S. Malik; "Summary of Information on Gamma Radiation from Atomic Weapons"; LA-1620, Jan 1954; Los Alamos Scientific Laboratory, Los Alamos, New Mexico; Secret Restricted Data.

7. G. W. Harding; "Permanent Reduction in Efficiency of Scintillation Materials Following Intense Gamma Radiation"; AERE N/M 51, Apr 1951.

8. R. H. Dempsey and others; "Gamma Radiation Dosimetry"; Project 2.1, Operation Castle, WT-912, May 1954; U. S. Army Signal Engineering Laboratories, Fort Monmouth, N. J.; Secret Restricted Data.

9. "The Nuclear Radiation Handbook"; AFSWP 1100, Mar 1957; Nuclear Development Corporation of America, White Plains, N. Y.; Secret Restricted Data.

DISTRIBUTION

Military Distribution Category 28

ARMY ACTIVITIES

1 Deputy Chief of Staff for Military Operations, D/A, Washington 25, D.C. ATTN: Dir. of SW&R
2 Chief of Research and Development, D/A, Washington 25, D.C. ATTN: Atomic Div.
3 Assistant Chief of Staff, Intelligence, D/A, Washington 25, D.C.
4- 5 Chief Chemical Officer, D/A, Washington 25, D.C.
6 Chief of Engineers, D/A, Washington 25, D.C. ATTN: ENGNB
7 Chief of Engineers, D/A, Washington 25, D.C. ATTN: ENGTB
8- 9 Office, Chief of Ordnance, D/A, Washington 25, D.C. ATTN: ORDTN
10 Chief Signal Officer, D/A, Comb. Dev. and Ops. Div., Washington 25, D.C. ATTN: SIGCO-4
11 The Surgeon General, D/A, Washington 25, D.C. ATTN: MEDNE
12- 14 Commanding General, U.S. Continental Army Command, Ft. Monroe, Va.
15 Director of Special Weapons Development Office, Headquarters CONARC, Ft. Bliss, Tex. ATTN: Capt. Chester I. Peterson
16 President, U.S. Army Artillery Board, U.S. Continental Army Command, Ft. Sill, Okla.
17 President, U.S. Army Air Defense Board, U.S. Continental Army Command, Ft. Bliss, Tex.
18 President, U.S. Army Aviation Board, Ft. Rucker, Ala. ATTN: ATBG-DG
19 Commandant, U.S. Army Command & General Staff College, Ft. Leavenworth, Kansas. ATTN: ARCHIVES
20 Commandant, U.S. Army Air Defense School, Ft. Bliss, Tex. ATTN: Dept. of Tactics and Combined Arms
21 Commandant, U.S. Army Armored School, Ft. Knox, Ky.
22 Commandant, U.S. Army Artillery and Missile School, Ft. Sill, Okla. ATTN: Combat Development Department
23 Commandant, U.S. Army Aviation School, Ft. Rucker, Ala.
24 Commandant, U.S. Army Ordnance School, Aberdeen Proving Ground, Md.
25 Commandant, U.S. Army Ordnance and Guided Missile School, Redstone Arsenal, Ala.
26 Commanding General, Chemical Corps Training Comd., Ft. McClellan, Ala.
27 Commanding General, The Engineer Center, Ft. Belvoir, Va. ATTN: Asst. Cmdt, Engr. School
28 Director, Armed Forces Institute of Pathology, Walter Reed Army Med. Center, 625 16th St., NW, Washington 25, D.C.
29 Commanding Officer, Army Medical Research Lab., Ft. Knox, Ky.
30 Commandant, Walter Reed Army Inst. of Res., Walter Reed Army Medical Center, Washington 25, D.C.
31- 32 Commanding General, QM R&D Comd., QM R&D Cntr., Natick, Mass. ATTN: CBR Liaison Officer
33 Commanding General, U.S. Army Chemical Corps, Research and Development Comd., Washington 25, D.C.
34 Commanding Officer, Chemical Warfare Lab., Army Chemical Center, Md. ATTN: Tech. Library
35 Commanding General, Engineer Research and Dev. Lab., Ft. Belvoir, Va. ATTN: Chief, Tech. Support Branch
36 Director, Waterways Experiment Station, P.O. Box 631, Vicksburg, Miss. ATTN: Library
37 Commanding Officer, Office of Ordnance Research, Box CM, Duke Station, Durham, North Carolina
38 Commanding Officer, Picatinny Arsenal, Dover, N.J. ATTN: ORDBB-TK
39 Commanding Officer, Diamond Ord. Fuze Labs., Washington 25, D.C. ATTN: Chief, Nuclear Vulnerability Br. (230)
40- 41 Commanding General, Aberdeen Proving Grounds, Md. ATTN: Director, Ballistics Research Laboratory
42 Commanding General, Frankford Arsenal, Bridge and Tacony St., Philadelphia, Pa.
43- 44 Commanding General, U.S. Army Ord. Missile Command, Redstone Arsenal, Ala.
45 Commander, Army Rocket and Guided Missile Agency, Redstone Arsenal, Ala. ATTN: Tech Library
46 Commanding General, White Sands Proving Ground, Las Cruces, N. Mex. ATTN: ORDBS-OM
47 Commander, Army Ballistic Missile Agency, Redstone Arsenal, Ala. ATTN: ORDAB-HT
48 Commanding Officer, Ord. Materials Research Off., Watertown Arsenal, Watertown 72, Mass. ATTN: Dr. Foster
49 Commanding General, Ordnance Tank Automotive Command, Detroit Arsenal, Centerline, Mich. ATTN: ORDMC-RO
50 Commanding Officer, USA Signal R&D Laboratory, Ft. Monmouth, N.J.
51 Commanding General, U.S. Army Electronic Proving Ground, Ft. Huachuca, Ariz. ATTN: Tech. Library
52 Commanding General, USA Combat Surveillance Agency, 1124 N. Highland St., Arlington, Va.
53 Commanding Officer, USA, Signal R&D Laboratory, Ft. Monmouth, N.J. ATTN: Tech. Doc. Ctr., Evans Area
54 Director, Operations Research Office, Johns Hopkins University, 6935 Arlington Rd., Bethesda 14, Md.
55 Commander-in-Chief, U.S. Army Europe, APO 403, New York, N.Y. ATTN: Opot. Div., Weapons Br.
56 Commanding Officer, 9th Hospital Center, APO 180, New York, N.Y. ATTN: CO, US Army Nuclear Medicine Research Detachment, Europe

NAVY ACTIVITIES

57 Chief of Naval Operations, D/N, Washington 25, D.C. ATTN: OP-03EG
58 Chief of Naval Operations, D/N, Washington 25, D.C. ATTN: OP-36
59 Chief of Naval Operations, D/N, Washington 25, D.C. ATTN: OP-922G2
60- 61 Chief of Naval Research, D/N, Washington 25, D.C. ATTN: Code 811
62- 63 Chief, Bureau of Aeronautics, D/N, Washington 25, D.C.
64 Chief, Bureau of Medicine and Surgery, D/N, Washington 25, D.C. ATTN: Special Wpns. Def. Div.
65 Chief, Bureau of Ordnance, D/N, Washington 25, D.C.
66 Chief, Bureau of Ordnance, D/N, Washington 25, D.C. ATTN: S.P.
67 Chief, Bureau of Ships, D/N, Washington 25, D.C. ATTN: Code 423
68 Chief, Bureau of Yards and Docks, D/N, Washington 25, D.C. ATTN: D-440
69 Director, U.S. Naval Research Laboratory, Washington 25, D.C. ATTN: Mrs. Katherine H. Cass
70- 71 Commander, U.S. Naval Ordnance Laboratory, White Oak, Silver Spring 19, Md.
72 Director, Material Lab. (Code 900), New York Naval Shipyard, Brooklyn 1, N.Y.
73 Commanding Officer and Director, Navy Electronics Laboratory, San Diego 52, Calif.
74- 77 Commanding Officer, U.S. Naval Radiological Defense Laboratory, San Francisco, Calif. ATTN. Tech. Info. Div.
78- 79 Officer-in-Charge, U.S. Naval Civil Engineering R&E Lab., U.S. Naval Construction Bn. Center, Port Hueneme, Calif. ATTN: Code 753
80 Commanding Officer, U.S. Naval Schools Command, U.S. Naval Station, Treasure Island, San Francisco, Calif.
81 Superintendent, U.S. Naval Postgraduate School, Monterey, Calif.
82 Officer-in-Charge, U.S. Naval School, CEC Officers, U.S. Naval Construction Bn. Center, Port Hueneme, Calif.

83 Commanding Officer, Nuclear Weapons Training Center, Atlantic, U.S. Naval Base, Norfolk 11, Va. ATTN: Nuclear Warfare Dept.

84 Commanding Officer, Nuclear Weapons Training Center, Pacific, Naval Station, San Diego, Calif.

85 Commanding Officer, U.S. Naval Damage Control Tng. Center, Naval Base, Philadelphia 12, Pa. ATTN: ABC Defense Course

86 Commanding Officer, Air Development Squadron 5, VX-5, China Lake, Calif.

87 Commander, Officer U.S. Naval Air Development Center, Johnsville, Pa. ATTN: NAS, Librarian

88 Commanding Officer, U.S. Naval Medical Research Institute, National Naval Medical Center, Bethesda, Md.

89-92 Commandant, U.S. Marine Corps, Washington 25, D.C. ATTN: Code A03H

93 Chief, Bureau of Ships, D/M, Washington 25, D.C. ATTN: Code 372

94 Commanding Officer, U.S. Naval CIC School, U.S. Naval Air Station Glynco, Brunswick, Ga.

AIR FORCE ACTIVITIES

95 Assistant for Atomic Energy, HQ, USAF, Washington 25, D.C. ATTN: DCS/O

96 Deputy Chief of Staff, Operations HQ. USAF, Washington 25, D.C. ATTN: Operations Analysis

97-98 Assistant Chief of Staff, Intelligence, HQ. USAF, Washington 25, D.C. ATTN: AFCIN-IB2

99 Director of Research and Development, DCS/D, HQ. USAF, Washington 25, D.C. ATTN: Guidance and Weapons Div.

100 The Surgeon General, HQ. USAF, Washington 25, D.C. ATTN: Bio.-Def. Pre. Med. Division

101 Commander-in-Chief, Strategic Air Command, Offutt AFB, Neb. ATTN: OAWS

102 Commander, Tactical Air Command, Langley AFB, Va. ATTN: Doc. Security Branch

103 Commander, Air Defense Command, Ent AFB, Colorado. ATTN: Atomic Energy Div., ADLAN-A

104 Commander, Hq. Air Research and Development Command, Andrews AFB, Washington 25, D.C. ATTN: RDRWA

105 Commander, Western Development Division (ARDC) P.O. Box 262, Inglewood, Calif. ATTN: WDSIT, Mr. R. O. Weitz

106-107 Commander, AF Cambridge Research Center, L. G. Hanscom Field, Bedford, Mass. ATTN: CRQST-2

108-112 Commander, Air Force Special Weapons Center, Kirtland AFB, Albuquerque, N. Mex. ATTN: Tech. Info. & Intel. Div.

113-114 Director, Air University Library, Maxwell AFB, Ala.

115 Commander, Lowry AFB, Denver, Colorado. ATTN: Dept. of Sp. Wpns. Tng.

116 Commandant, School of Aviation Medicine, USAF, Randolph AFB, Tex. ATTN: Research Secretariat

117 Commander, 1009th Sp. Wpns. Squadron, HQ. USAF, Washington 25, D.C.

118-119 Commander, Wright Air Development Center, Wright-Patterson AFB, Dayton, Ohio. ATTN: WCOSI

120-121 Director, USAF Project RAND, VIA: USAF Liaison Office, The RAND Corp., 1700 Main St., Santa Monica, Calif.

122 Commander, Air Defense Systems Integration Div., L. G. Hanscom Field, Bedford, Mass. ATTN: SIDE-S

123 Chief, Ballistic Missile Early Warning Project Office, 220 Church St., New York 13, N.Y. ATTN: Col. Leo V. Skinner, USAF

124 Assistant Chief of Staff, Intelligence, HQ. USAFE, APO 633, New York, N.Y. ATTN: Directorate of Air Targets

125 Commander-in-Chief, Pacific Air Forces, APO 953, San Francisco, Calif. ATTN: PFOIE-MB, Base Recovery

OTHER DEPARTMENT OF DEFENSE ACTIVITIES

126 Assistant Secretary of Defense, Research and Engineering, DOD, Washington 25, D.C. ATTN: Tech. Library

127 Director, Weapons Systems Evaluation Group, Room 1E880, The Pentagon, Washington 25, D.C.

128-135 Chief, Armed Forces Special Weapons Project, Washington 25, D.C.

136 Commander, Field Command, AFSWP, Sandia Base, Albuquerque, N. Mex.

137 Commander, Field Command, AFSWP, Sandia Base, Albuquerque, N. Mex. ATTN: FCTG

138-142 Commander, Field Command, AFSWP, Sandia Base, Albuquerque, N. Mex. ATTN: FCWT

143 Commander, JTF-7, Arlington Hall Station, Arlington 12, Va.

144 U.S. Documents Officer, Office of the United States National Military Representative - SHAPE, APO 55, New York, N.Y.

ATOMIC ENERGY COMMISSION ACTIVITIES

145-147 U.S. Atomic Energy Commission, Technical Reports Library, Washington 25, D.C. ATTN: Mrs. J. M. O'Leary (For DMA)

148-149 Los Alamos Scientific Laboratory, Report Library, P.O. Box 1663, Los Alamos, N. Mex. ATTN: Helen Redman

150-154 Sandia Corporation, Classified Document Division, Sandia Base, Albuquerque, N. Mex. ATTN: H. J. Smyth, Jr.

155-157 University of California Radiation Laboratory, P.O. Box 808, Livermore, Calif. ATTN: Clovis G. Craig

158 Weapon Data Section, Technical Information Service Extension, Oak Ridge, Tenn.

159-195 Technical Information Service Extension, Oak Ridge, Tenn. (Surplus)

Unclassified

UNCLASSIFIED

AD 338330

CLASSIFICATION CHANGED
TO: UNCLASSIFIED
FROM: SECRET -Rd
AUTHORITY: DNA
ltr, 12 Dec 80

UNCLASSIFIED

UNCLASSIFIED

AD 338330

DEFENSE DOCUMENTATION CENTER

FOR

SCIENTIFIC AND TECHNICAL INFORMATION

CAMERON STATION, ALEXANDRIA, VIRGINIA

NOTICE: When government or other drawings, specifications or other data are used for any purpose other than in connection with a definitely related government procurement operation, the U. S. Government thereby incurs no responsibility, nor any obligation whatsoever; and the fact that the Government may have formulated, furnished, or in any way supplied the said drawings, specifications, or other data is not to be regarded by implication or otherwise as in any manner licensing the holder or any other person or corporation, or conveying any rights or permission to manufacture, use or sell any patented invention that may in any way be related thereto.

<u>NOTICE:</u>

THIS DOCUMENT CONTAINS INFORMATION AFFECTING THE NATIONAL DEFENSE OF THE UNITED STATES WITHIN THE MEANING OF THE ESPIONAGE LAWS, TITLE 18, U.S.C., SECTIONS 793 and 794. THE TRANSMISSION OR THE REVELATION OF ITS CONTENTS IN ANY MANNER TO AN UNAUTHORIZED PERSON IS PROHIBITED BY LAW.

UNCLASSIFIED/UNLIMITED